Microchimica Acta (2022) 189:396
https://doi.org/10.1007/s00604-022-05487-z

ORIGINAL PAPER

Nanomaterial-based sandwich-type electrochemical aptasensor platform for sensitive voltammetric determination of leptin

Cem Erkmen[1,2] · Gözde Aydoğdu Tığ[3] · Bengi Uslu[1]

Received: 28 June 2022 / Accepted: 6 September 2022 / Published online: 29 September 2022

Abstract

A sandwich-type electrochemical aptasensor was designed for sensitive detection of leptin in biological samples, including human serum and human plasma. The developed aptasensor was produced by electrodeposition of gold nanoparticles on a screen-printed electrode modified with zinc oxide nanoparticles. The synergy effect of zinc oxide and gold nanoparticles improved the electrocatalytic activity of the aptasensor. The obtained high surface area allowed more aptamer molecules to be loaded on the electrode surface. Signal amplification significantly increases the detection sensitivity of a developed biosensor. Although the use of nanomaterials is the most preferred detection tool for this purpose, as an alternative, enzyme-catalyzed signal amplification is widely used in the construction of a biosensor due to its specificity and high catalytic efficiency. Therefore, both nanomaterial-supported and an alkaline phosphatase-based aptasensor design were developed, which can produce in situ electroactive product by enzymatic hydrolysis of the inactive substrate to achieve a higher signal-to-background ratio. Under optimal conditions, the developed aptasensor exhibited a wide linear concentration range from 0.01 pg mL^{-1} to 100.0 pg mL^{-1} with a detection limit of 0.0035 pg mL^{-1}. While the developed aptasensor provided excellent selectivity in the presence of some interfering compounds, it possessed outstanding reproducibility and stability. In addition, the developed aptasensor has been applied with good recoveries in the range 96.31 to 108.79% in human serum and plasma samples. In conclusion, all the obtained results showed the feasibility of the developed aptasensor for practical applications.

Keywords Aptasensor · Differential pulse voltammetry · Gold nanoparticles · Leptin · Zinc oxide nanoparticles

Introduction

Traumatic brain injury (TBI), with approximately 69 million diagnoses per year, is a major health problem worldwide. A physical blow from an external factor, exposure to an explosion, slowing or stopping of the functions of brain cells, and difficulties caused by skull penetration cause TBI. TBI causes many neurodegenerative disorders in individuals and may decrease survivors' quality of life and increase the risk of developing chronic behavioral and neurological disorders. A study showed that more than 400,000 US military personnel were diagnosed with TBI between 2000 and 2019 due to the frequent exposure of military personnel to explosions [1–3]. Literature studies have reported that it involves the release of different cytokines, biological markers, and many neurotransmitters that contribute to the tissue damage process after TBI. The heterogeneous nature of TBI limits the complete understanding of its pathophysiology. Therefore, better diagnostic methods are needed to diagnose TBI. At this stage, biomarkers help determine the clinical diagnosis of TBI. Mainly, leptin is the hormone secreted by the adipocyte, which plays a vital role in regulating body weight and metabolism. However, research studies have revealed that leptin and its receptors act as a neuroprotective biomarker in neurodegenerative diseases and brain trauma [4–6]. Therefore, diagnosing and detecting leptin at low and initial concentrations is one of the essential strategies

✉ Gözde Aydoğdu Tığ
gaydogdu@science.ankara.edu.tr

✉ Bengi Uslu
buslu@pharmacy.ankara.edu.tr

[1] Department of Analytical Chemistry, Faculty of Pharmacy, Ankara University, 06560 Ankara, Turkey

[2] The Graduate School of Health Sciences, Ankara University, 06110 Ankara, Turkey

[3] Department of Chemistry, Faculty of Science, Ankara University, 06100 Ankara, Turkey

for neurodegenerative diseases and brain trauma in the early term.

At present, biosensor-based electrochemical methods provide fast response, high sensitivity, and low cost for analyzing various biological molecules. These properties attract the attention of researchers for the development of electrochemical immunosensors and enzyme sensors for the determination of biological molecules. However, immunosensors based on the interaction between antibody and antigen and enzyme sensors based on the interaction between enzyme-substrate have disadvantages. These include poor stability of antibodies and enzymes at high temperatures and relatively high cost. Aptamers are oligonucleotide sequences, such as DNA or RNA, with selectivity towards the target analyte, determined in vitro by the systematic evolution of ligands by exponential enrichment (SELEX) method. Recently, aptamers have attracted increased interest in sensor studies due to their strong antigen-binding affinity, easy synthesis, high stability under different environmental conditions, low cost, smaller size 20–25 fold smaller than antibodies, low immunogenicity, and easy functionalization. However, the small current responses of the electrochemical aptasensor still limit their sensitivity. Therefore, nanomaterials as labels play an essential role in increasing the sensitivity of electrochemical aptasensors, as they can effectively amplify the current signal [7–10].

Among various nanomaterials, zinc oxide nanoparticles (ZnO NPs), a wide-bandgap semiconductor, have attracted interest in biosensor platforms due to their desirable properties such as non-toxicity stable nanostructures, good biocompatibility, high surface area, and high electron transfer efficiency. Therefore, ZnO NPs are also a good candidate for constructing aptasensor platforms [11]. Gold nanoparticles (Au NPs) are the most frequently used nanomaterials. Due to their low density, effective surface area, exchange mass transfer, catalytic facilitation, and conductivity, Au NPs have potential applications in a variety of sensors design. Molecules with functional groups such as $–NH_2$ and –SH can bind to Au NPs and lead to chemical stability and strong adherence of molecules to the electrode surface. Therefore, Au NPs, due to their unique properties, have been at the forefront of their sensor applications, including oligonucleotides, proteins, and antibodies based. Moreover, the combination of highly conductive noble metal Au NPs with ZnO NPs is an ideal platform for utility and enhancing the performance of the electrochemical sensor [12–14].

The charge transfer characteristics of ZnO NPs, a semiconductor material, are limited. Therefore, modifying ZnO NPs with noble metal NPs and using these composites in sensor architecture is an easy and effective option to increase the conductivity of ZnO NPs. Noble metal NPs such as Pt, Pd, and Au are frequently combined with ZnO NPs to increase catalytic property and conductivity. Among them, the combination of ZnO NPs and Au NPs has been widely preferred due to its doped redox property, excellent stability, and high electrical conductivity during electrochemical reactions. In addition, it was observed that the active sites and specific surface area of ZnO NPs increased with the composite materials composed of ZnO NPs and Au NPs. Therefore, developed sensors by taking advantage of the high surface area of ZnO NPs and high-density conductive Au NPs can exhibit sensitive results with a lower detection limit and wider linear range [15–17].

Among various amplification strategies, enzyme-amplified assay strategies and nanomaterial-based amplified assay strategies have been utilized to improve the detection sensitivity of the developed sensors. Especially, enzyme-amplified assay strategies stand out as the most commonly used strategy due to their simplicity, good reproducibility, and ability to detect ultra-low concentrations of biological molecules. Among the different enzymatic markers, horseradish peroxidase (HRP), glucose oxidase (GOx), and alkaline phosphatase (ALP) are the most commonly used markers in enzyme-amplified detection systems in connection with electrochemical monitoring of the biocatalytic reaction product [18–21].

In this novel aptasensor, we presented a sandwich-type electrochemical aptasensor using Au NPs/ZnO NPs as loading aptamer molecules for highly sensitive detection of leptin. Au NPs/ZnO NP-modified surface provides ample surface area, abundant porous structure, good conductivity, and synergistic catalysis towards ALP could effectively amplify the signal. Under optimal experimental conditions, the detection of leptin was investigated by differential pulse voltammetry (DPV). Validation parameters including linear range, detection limit, selectivity, stability and reproducibility were evaluated. Additionally, the developed aptasensor was also used to detect leptin in real samples such as human serum and human plasma to indicate potential practical utilization in the clinical diagnosis. To the best of our knowledge, this research is the first report of an ultrasensitive sandwich-type leptin aptasensor that ALP was used for enzyme-amplified by performed on Au NPs/ZnO NP-modified screen-printed electrode (SPE) surface.

Materials and methods

Materials and reagents

In this study, leptin as a relevant biomarker, ZnO NPs and tetrachloroauric acid ($HAuCl_4 \cdot 3H_2O$) used for electrode modification were purchased from Sigma–Aldrich. To prepare buffers and solutions used in experimental studies, $K_3Fe(CN)_6 \cdot 3H_2O$, $K_4Fe(CN)_6 \cdot 3H_2O$, KCl, $MgCl_2$, NaCl, TRIS HCl, EDTA, diethanolamine (DEA) and

6-mercapto-1-hexanol (6-MCH) were supplied from Sigma–Aldrich. Streptavidin-alkaline phosphatase (Strep-ALP), and α-naphthyl phosphate were purchased from Sigma-Aldrich. Real biological samples of human serum (from human male AB plasma) and human plasma were purchased from Sigma–Aldrich. Interfering compounds including L-lysine, haptoglobin, dopamine, ascorbic acid, paracetamol human serum albumin (HSA), and bovine serum albumin (BSA) were supplied from Sigma–Aldrich. All reagents and chemicals used in the studies were of analytical grade. Ethanol was of chromatographic quality and obtained from Merck KGaA.

The DNA aptamer sequences which are specific for leptin was determined by a previous study [22]. The thiolated primary aptamer and biotinylated secondary aptamer were supplied from Metabion GmbH, and the sequences of these aptamers were of:

Thiolated Apt1:

5 ´-SH-$(CH_2)_6$-GTTAATGGGGGATCTCGCGGCCGTTCTTGTTGCTTATACA-3´.

Biotinylated Apt2:

3´-(Biotin)-(Triethylene glycol)-CAATTACCCCCTAGAGCGCCGGCAAGAACAACGAATATGT-5′.

Instruments

In this study, the commercial SPE (DRP-C110) 3-mm diameter was used to develop an aptasensor (Metrohm, DropSens, Turkey). The SPE consists of carbon, silver, and carbon as working, reference, and auxiliary electrodes, respectively. To obtain electrochemical signals using cyclic voltammetry (CV), DPV, and electrochemical impedance spectroscopy (EIS), Autolab PGSTAT 302 N potentiostat/galvanostat electrochemical analyzer. Nova 2.1.2 software (Eco Chemie, The Netherlands) was used to obtain all electrochemical signals. Pulse amplitude, step potential, modulation time, interval time, and scan rate values were set as 50 mV, 3 mV, 0.02 s, 0.2 s, and 15 mV s^{-1}, respectively, for experimental conditions of the DPV method. EIS measurements were performed by amplitude 10 mV and the frequency in the range of 10 kHz to 0.01 Hz. The experimental data were obtained by fitting the impedance plots to an equivalent circuit. All electrochemical measurements were performed at ambient conditions (25 °C). ORION 720 A pH meter and PURELAB Option-Q system were used to determine the pH of the prepared buffer solutions and other solutions and to obtain double distilled water, which is used to prepare all solutions, respectively. The surface morphology of the nanomaterial and aptamer modified electrodes were investigated by SEM images obtained from ZEISS EVO 40/Merlin, Carl Zeiss (Oberkochen, Germany). The X-ray diffraction (XRD) pattern of Au NPs, ZnO NPs, and Au NPs/ZnO NPs were investigated by an APD 2000 PRO diffractometer using Cu-Kα radiation in θ–2θ configuration.

Preparation of modified electrode

The preparation process of Au NPs/ZnO NPs/SPE was based on a layer-by-layer modification procedure. After 0.25 mg mL^{-1} of ZnO NPs were dispersed in ethanol, 10 µL of ZnO NP suspension was dropped on the surface of SPE and allowed to dry at room temperature. In the second step, electrodeposition of Au NPs onto the ZnO NP-modified SPE surface was performed according to previous studies. To obtain Au NPs/ZnO NPs/SPE, the CV method [23, 24] was used in a potential range of −0.3 +1.2 V and 50 mV s^{-1} was the scan rate. After Au NPs were covered by successive 15 cycles at KCl solution, including 1.0 mM $HAuCl_4$, the modified surface was cleaned with double distilled water and allowed to dry for the following modification steps.

Construction of sandwich-type aptasensor

The construction steps of sandwich-type aptasensor for leptin detection are schematized in Scheme 1. Firstly, the ZnO NPs/SPE and Au NPs/ZnO NPs/SPE were prepared as described in the previous step. Then, 10 µL of 0.5 µM thiol-tethered DNA aptamer (Apt1) were incubated onto the surface of Au NPs/ZnO NP-modified SPE. To prevent evaporation of the dropped Apt1 solution, the electrodes were kept at +4 °C overnight in a Petri dish for efficient binding of aptamers with Au NPs and to allow the formation of Au-S self-assembled monolayers. After the Apt1 solution was removed from the surface, the electrode was washed using TRIS-HCl buffer (20 mM, pH 7.4), which consisted of 0.1 M NaCl, 0.1 M KCl, and 0.05 M $MgCl_2$. Then, to prevent non-specific interactions, 1.0 mM 6-MCH solution was dropped on the Apt 1 modified surface, and after it was left for 1 hour, the electrode was washed three times with TRIS-HCl buffer.

In a further step, 10 µL of dropped leptin solution at increasing concentrations was immobilized onto the aptasensor surface for 30 min and then washed with TRIS-HCl buffer (20 mM, pH 7.4). To fabricate a sandwich-type aptasensor, the 10 µL of 1.5 µM biotinylated aptamer (Apt2) was incubated on the leptin/Apt1/Au NPs/ZnO NPs/SPE for 30 min. The aptasensor was rinsed with TRIS-HCl (pH 7.4). Then, the mixture of 10 µL of 1 U mL^{-1} Strep-ALP solution and 10 mg mL^{-1} BSA in 0.1 M DEA buffer (pH 9.6) was dropped onto the surface of Apt2/leptin/Apt1/Au NPs/ZnO NPs/SPE for 20 min. Before proceeding to the final step, the aptasensor was rinsed with 0.1 M DEA buffer.

In the final step, 1 mg mL^{-1} of α-naphthyl phosphate was prepared in 0.1 M DEA buffer, and 60 µL of this enzymatic substrate was dropped on the Apt2/leptin/Apt1/Au NPs/

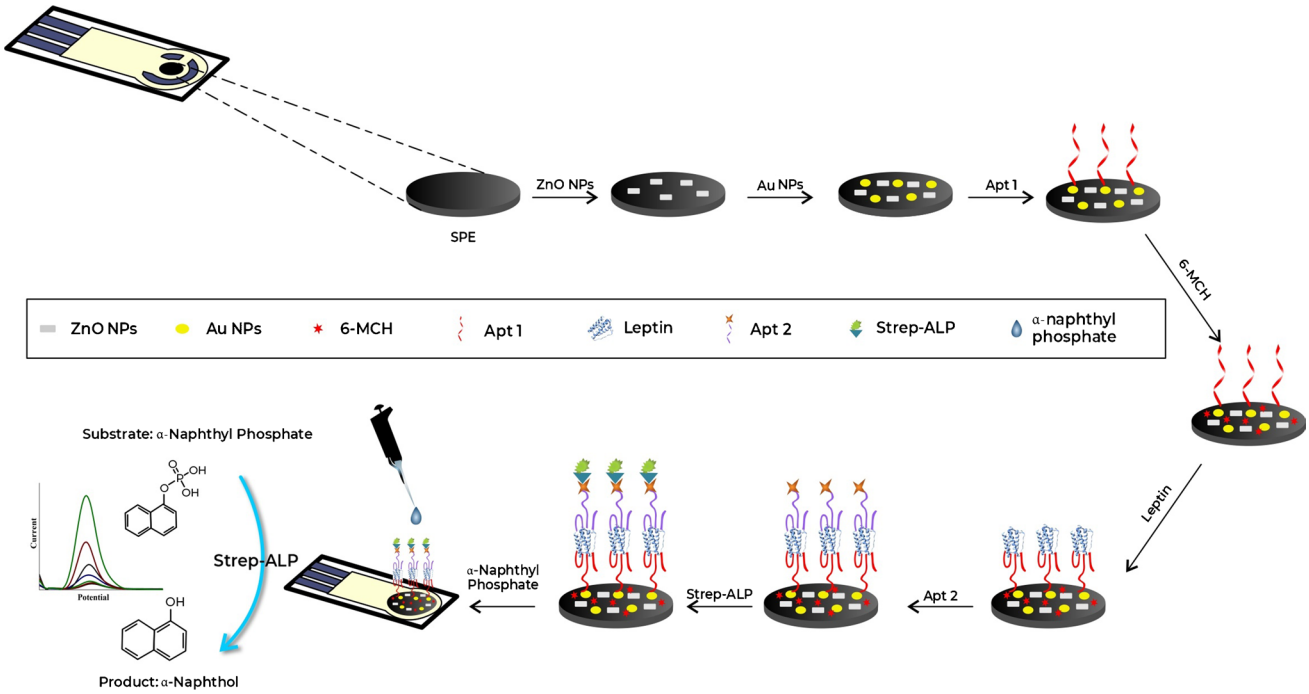

Scheme 1 Schematic representation of the developed aptasensor

ZnO NPs/SPE surface for 20 min. Analytical responses were recorded by monitoring the DPV responses of α -naphthol, an electroactive product formed after the interaction, in the potential range of ⁻0.2 V and +0.35 V.

Application of the leptin aptasensor

The ability of the developed aptasensor was checked by determining leptin content in human serum and human plasma samples. Based on the standard addition method, three different leptin concentrations were added to real samples diluted 1:10. The recovery% values were calculated using the regression equations related to the current values obtained by the DPV. Each spiked serum and plasma samples were studied based on three parallel measurements with the developed aptasensor.

Results and discussion

Characterization of the leptin aptasensor

The morphological structure of the prepared nanomaterial modified sensors and aptasensor was elucidated by SEM and EDX analysis. The bare SPE (Fig. 1A) exhibits a relatively smooth carbon layer surface. The SEM image of ZnO NPs/SPE clearly shows spherical porous structures evenly distributed on SPE, as seen in Fig. 1B [25, 26]. As can be noticed in Fig. 1C, the electrochemical deposition of Au NPs was a very effective method leading to a homogeneous and uniform distribution of Au NPs on the SPE [27]. After electrodepositing Au NPs on the surface of ZnO NPs/SPE (Fig. 1D), Au NPs were uniformly whiter dispersed and spherical on the surface [28, 29]. Moreover, Fig. 1E showed the backscattering image of the Au NPs/ ZnO NPs/SPE. The brightly lit particles were Au NPs whereas the dim particle sat in the background was ZnO NPs. This is because of the heavier mass of the Au NPs compared to the ZnO NPs. As seen in Fig. 1F, the electrode surface morphology changed after the aptamer molecules were immobilized onto the surface. The resulting surface structure confirmed the immobilization of the aptamer to the surface, as seen in previous studies [30–32]. In addition, the elemental analysis results obtained from the EDX spectrum confirmed that there were 60% ZnO NPs and 20% Au NPs from the Au NPs/ZnO NPs/SPE surface (Fig. S1A). As seen in Fig. S1B, the presence of 10% by weight nitrogen indicated successful immobilization of aptamer molecules on the surface.

Furthermore, the crystallographic structure of the prepared Au NPs/ZnO NP-modified electrode for the developed aptasensor was characterized using XRD. As can be seen in Fig. S2A, the diffraction peaks of 38.3°, 44.4°, and 64.4° at 2θ can be related to the (111), (200), and (220) planes of Au NPs, respectively. The obtained results showed that the SPE surface was successfully coated with metallic Au NPs by the electrodeposition using the $HAuCl_4$ precursor [33, 34].

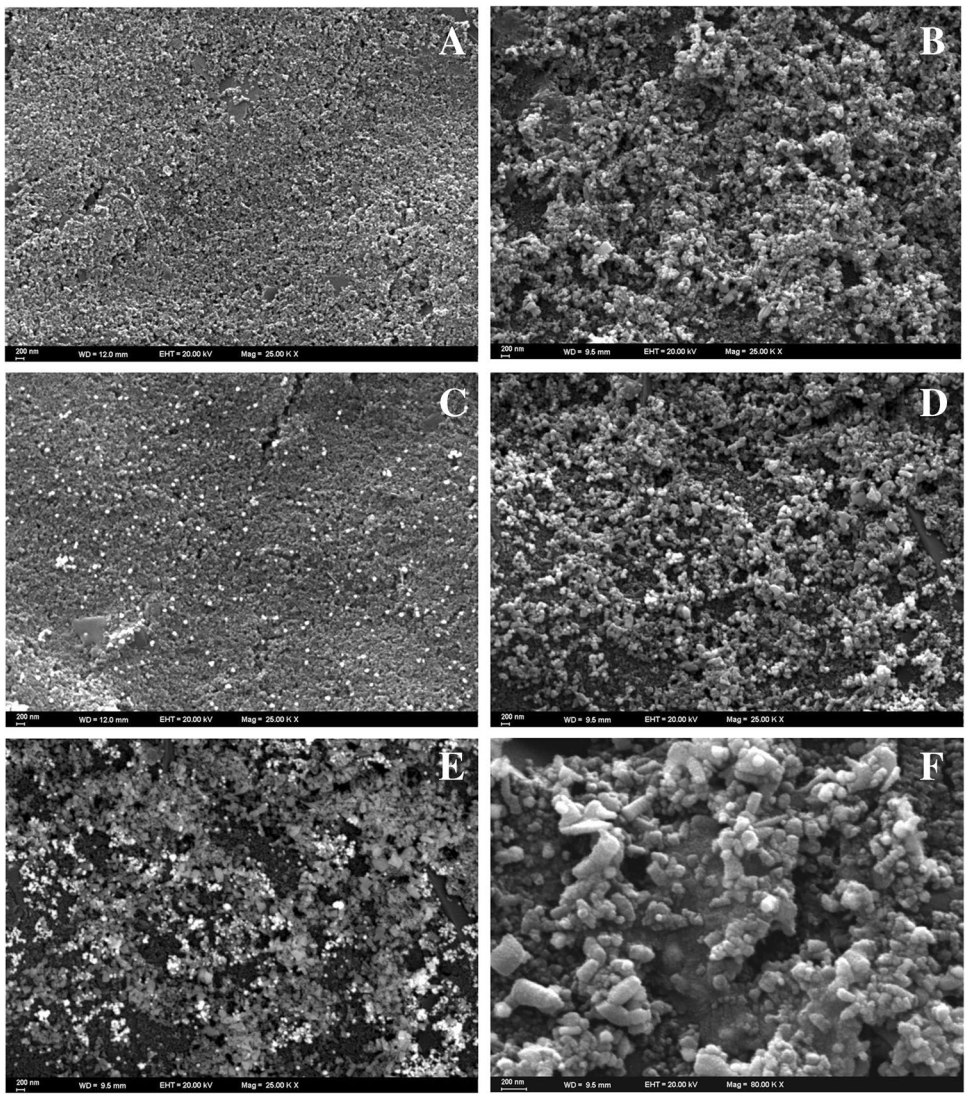

Fig. 1 SEM images of bare SPE (**A**), ZnO NPs/SPE (**B**), Au NPs/SPE (**C**), Au NPs/ZnO NPs/SPE (**D**), backscattered electron SEM images of Au NPs/ ZnO NPs/SPE (**E**) "images were taken at 25.00 magnitudes," and Apt1/Au NPs/ZnO NPs/SPE (**F**) "image was taken at 80.00 magnitudes"

Also, XRD pattern of ZnO NPs was shown in Fig. S2B. The observed peaks at 2θ = 31.8, 34.5, 36.3, 47.6, 56.8, 63.0, and 68.7 confirmed that the (100), (002), (101), (102), (110), (103), and (112) planes of hexagonal ZnO NP structure, respectively [35, 36]. Moreover, the XRD pattern results obtained in the presence of both ZnO NPs and Au NPs on the SPE surface reveal that there are no additional peaks in the diffraction pattern. It can conclude that the prepared modified electrode has an excellent purity (Fig. S2C).

Electrochemical characterization of the leptin aptasensor

The first and most crucial step of the sensor studies is to examine the characterization of the designed sensor platforms at each modification step [37, 38]. For this purpose, CV and EIS methods were performed to investigate the electrochemical behaviors of prepared electrodes in 5.0 mM redox solution containing 0.1 M KCl. As seen in Fig. 2A, the anodic peak current of ZnO NP-modified SPE (98.77 µA) was more significant than bare SPE (80.19 µA). This increase in current value indicates that ZnO NPs can support direct electron transfer between the redox molecule and the electrode. After the SPE surface was modified with Au NPs, the high conductivity and excellent electrocatalytic properties of Au NPs allowed the current value to increase up to 116.00 µA [39, 40]. Moreover, Au NPs/ZnO NPs/SPE had the highest peak current (162.22 µA) while simultaneously shifting the peak potential to a more negative potential of 127 mV. This can be attributed to the electrochemical catalytic activity of Au NPs and the synergistic effect between Au NPs and ZnO NPs [12, 41]. Then, when thiolated Apt1 was immobilized on the surface of Au NPs/ZnO NPs/SPEs, Apt1 molecules could bind via Au-S covalent bonds. The current value of the Apt1 modified sensor decreased to 113.77 µA, indicating that the aptamers were successfully

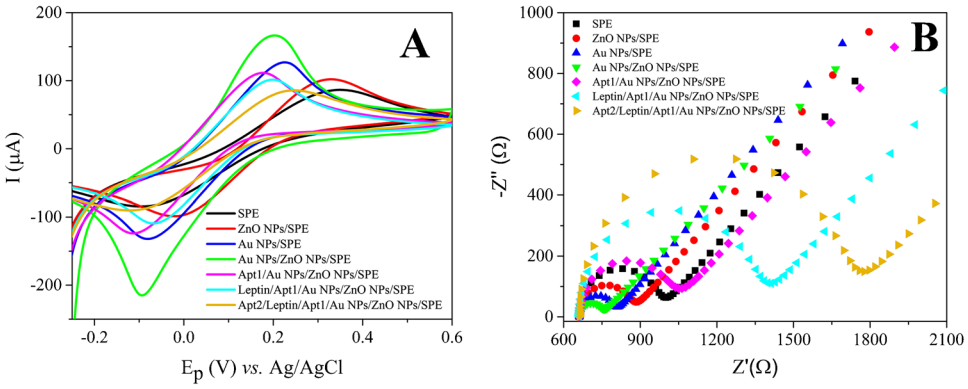

Fig. 2 CV (**A**) and EIS (**B**) graphs of bare SPE, ZnO NPs/SPE, Au NPs/SPE, Au NPs/ZnO NPs/SPE, Apt1/Au NPs/ZnO NPs/SPE, leptin/Apt1/Au NPs/ZnO NPs/SPE, and Apt2/leptin/Apt1/Au NPs/ZnO NPs/SPE in 0.1 M KCl solution containing 5.0 mM $Fe(CN)_6^{3-/4-}$

immobilized on the electrode surface. Subsequently, after incubation with leptin, the current value (100.21 μA) decreased further due to the non-electroactive property of leptin. Finally, when biotinylated Apt2 was immobilized onto the leptin/Apt1/Au NPs/ZnO NPs/SPE surface, the decrease in current value (75.20 μA) continued with the inhibition of electron transfer by aptamer molecules [42, 43]. Moreover, it can be seen that the high specific surface area of Au NPs/ZnO NPs/SPE (0.195 cm^2) compared with the electrochemical surface area of bare SPE (0.097 cm^2) can better immobilize the Apt1 molecule onto the surface, thus effectively improving the performance of leptin aptasensor (Detailed calculations are available in supplementary files, in Fig. S3, and Table S1).

The electron transportability of the modified electrodes was determined by charge transfer resistance (R_{ct}) values obtained by the EIS measurements. As seen in Fig. 2B, the R_{ct} values of unmodified SPE, ZnO NPs/SPE, Au NPs/SPE, and Au NPs/ZnO NPs/SPE were found to be 305.0 Ω, 199.0 Ω, 134.0 Ω, and 56.0 Ω, respectively. Thanks to the semiconductor properties of ZnO NPs and the excellent conductivity of Au NPs, the decrease in R_{ct} value indicates that Au NPs/ZnO NPs/SPE was a suitable surface for the immobilization of aptamer molecules. After successfully immobilizing Apt1, leptin, and Apt2 molecules onto surfaces, R_{ct} values increased to 390.0 Ω, 696.0 Ω, and 1030.0 Ω, respectively. These increases in R_{ct} values can be attributed to the fact that electron transfer is inhibited by the densely packed aptamer and leptin molecules [44, 45]. As a result, all CV and EIS (Table S1) responses showed that the proposed aptasensor was successfully fabricated for leptin detection.

Optimization of electrode modification

The first factor that strongly affects the sensing performance of the proposed aptasensor is the successful immobilization of the aptamer molecule to the surface. For this reason, the concentration of ZnO NPs and the number of cycles during the electrodeposition of Au NPs were optimized by the EIS method. Firstly, the amount of ZnO NPs varied between 0.10 and 1.0 mg mL^{-1}. As seen in Fig. 3A, the presence of 0.10 mg mL^{-1} of ZnO NPs on the electrode surface caused a decrease in the R_{ct} of the electrode surface, while 0.5 mg mL^{-1} and 1.0 mg mL^{-1} of ZnO NPs increased the R_{ct}. The R_{ct} value continued to increase significantly when the amount of ZnO NPs exceeded 0.25 mg mL^{-1}. This phenomenon can be attributed to the thick layers that appear on the modified electrode surface, which block the electron transfer pathway and prevent electrons from reaching the electrode surface, thus causing a decrease in sensitivity. As a result,

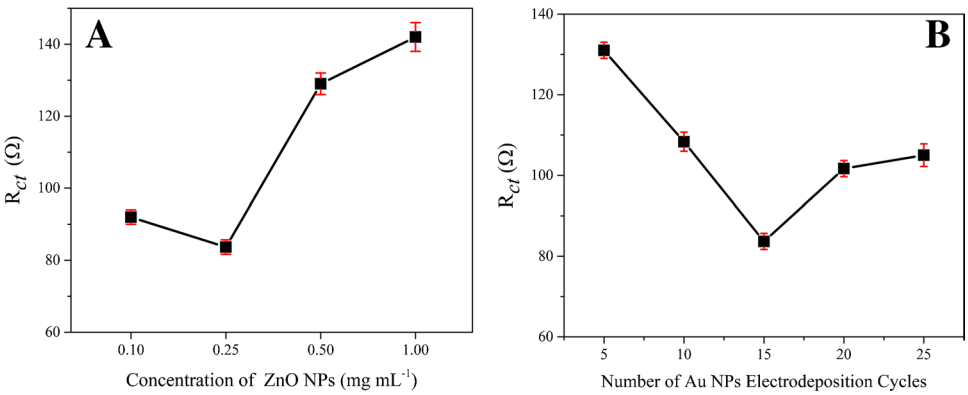

Fig. 3 The effect of ZnO NP (**A**) concentration and the number of Au NP electrodeposition cycles on the EIS signal of the 0.1 M KCl solution containing 5.0 mM $Fe(CN)_6^{3-/4-}$

0.25 mg mL^{-1} ZnO NPs facilitated charge transfer on the electrode surface, causing an observable reduction in charge transfer resistance. The cycle number of electrodeposition affects the size and distribution of Au NPs onto the electrode surface [17]. Therefore, as another parameter, the number of cycles for the electrodeposition was changed between 5 and 25. As shown in Fig. 3B, the R_{ct} value showed a decreasing trend when the number of cycles was changed from 5 to 15, and after 15 cycles, the R_{ct} value showed an increasing trend. The higher cycles than 15 cycles cause more extensive electrodeposition of Au NPs, and the formation of a thicker film with less accessible surface sites and low conductivity occurs. These results showed that the aptamer molecules could be successfully immobilized on the electrode surface coated with 0.25 mg mL^{-1} ZnO NPs and 1.0 mM Au NPs for 15 cycles. Therefore, this concentration and the number of cycles were chosen as optimal values and used for subsequent experiments.

Electrochemical behavior and optimization of conditions

To check the feasibility of the signal amplification strategy, the current response of α-naphthol toward leptin was investigated at different electrodes. As indicated in Fig. 4, a current response of 0.07 µA was obtained when no nanomaterial existed on the SPE surface. When the SPE surface was modified with ZnO NPs and Au NPs, the current values were 0.30 µA and 3.75 µA, respectively. While the ZnO NPs and Au NPs existed on the electrode surface, the current value increased by 220.0% (15.4 µA) compared with other electrodes. These results explained that ZnO NPs and Au NPs could further promote the conductivity of the aptasensor.

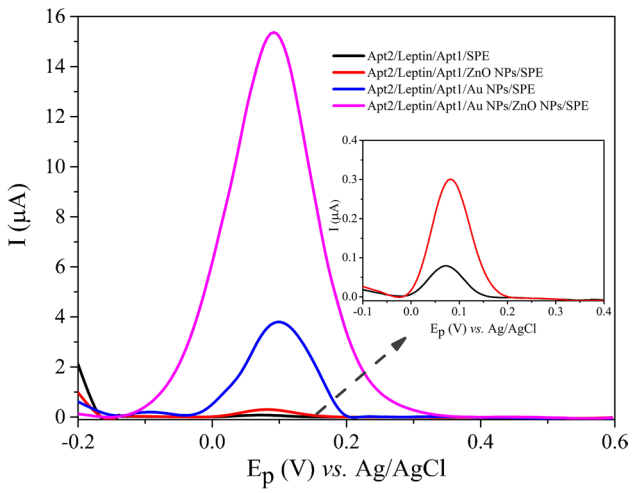

Fig. 4 DPV signal of the α-naphthol at Apt2/leptin/Apt1/SPE, Apt2/leptin/Apt1/ZnO NPs/SPE, Apt2/leptin/Apt1/Au NPs/SPE, and Apt2/leptin/Apt1/Au NPs/ ZnO NPs/SPE

Furthermore, the significant increase in current indicates that the combination of ZnO NPs and Au NPs allowed for more immobilization of aptamer and leptin molecules on the electrode surface [46].

In this study, some critical experimental factors were optimized for the developed aptasensor to exhibit the best performance for the leptin analysis. Firstly, the effect of different concentrations of Apt1 on the current response of α-naphthol varied from 0.05 to 2.0 µM. As seen in Fig. 5A, with increasing Apt1 concentration, the current signal increased up to 0.5 µM Apt1 and then remained saturated current value. Therefore, the optimum Apt1 concentration was determined as 0.5 µM for subsequent experiments. As a second parameter, the immobilization time of Apt2 was examined. As shown in Fig. 5B, the current signal showed an increasing trend from 5 min to 30 min, reaching equilibrium after 30 min. These results showed that the optimum immobilization time of Apt2 was 30 min.

Additionally, the effect of Apt2 concentration on leptin detection was investigated between 0.5 and 3.0 µM. Figure 5C shows that the highest current value was obtained at 1.5 µM Apt2 concentration, which can be selected as the optimum value. Moreover, the binding time of leptin was investigated as a final important parameter affecting the performance of the aptasensor. To optimize the binding time, 50.0 pg mL^{-1} leptin was incubated on the surface for between 5 and 60 min (Fig. 5D). While the current signal continued to increase up to 30 min, after 30 min, the aptamer molecules and leptin entirely interacted and showed saturation behavior. Therefore, it can be suggested that the optimal binding time of leptin for the proposed aptasensor was 30 min.

Analytical response of the leptin aptasensor

The analytical performance of the developed sandwich-type aptasensor was investigated by probing the dependence of the current response of α-naphthol on increasing leptin concentration. Figure 6A and B show DP voltammograms of α-naphthol at increasing leptin concentrations under optimum conditions. It can be seen that the current value gradually increases with an increase in leptin concentration. Using the developed aptasensor, good linearities (R^2> 0.99) were obtained between the values of peak currents and leptin concentration in two linear ranges from 0.01 to 5.0 pg mL^{-1} (Fig. 6C) and 5.0 to 100.0 pg mL^{-1} (Fig. 6D), respectively. The obtained linear regression equations were of I (µA) = 1.69 C_{Leptin} [pg mL^{-1}] +0.46 (R^2 = 0.998) and I (µA) =0.14 C_{Leptin} [pg mL^{-1}] +8.12 (R^2 = 0.999). This was not surprising as several published reports have shown two linear ranges at different concentrations in electrochemical investigations [47, 48]. Therefore, the two linear ranges observed in this study can be described by two factors. At

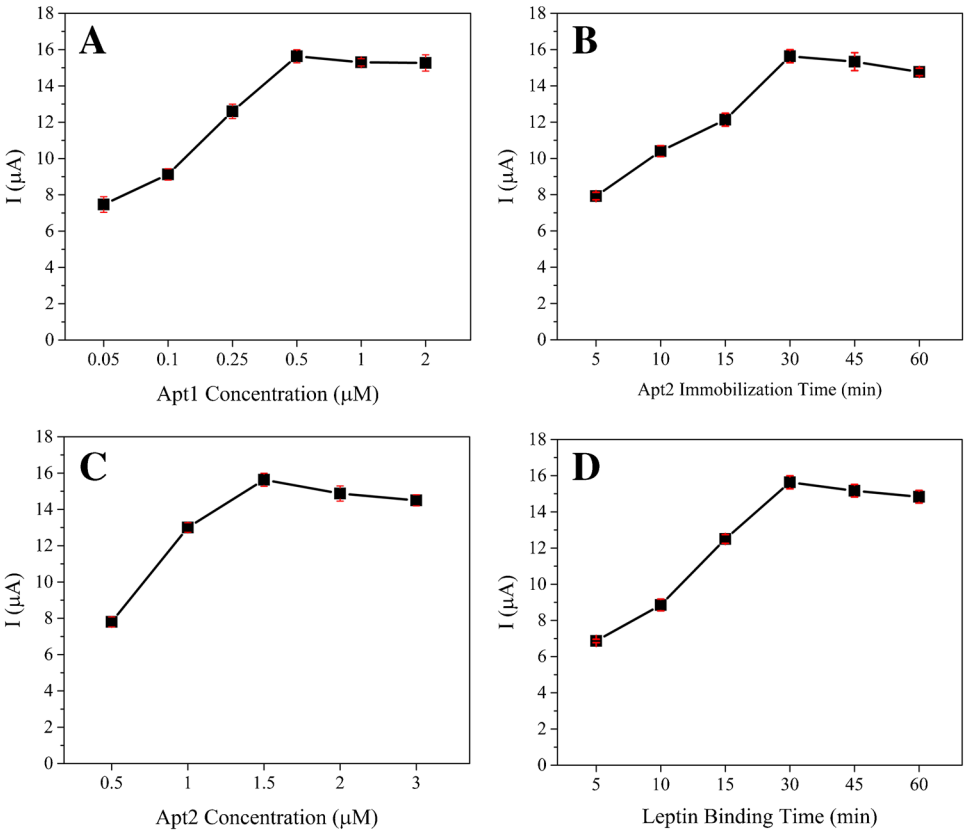

Fig. 5 The effect of concentration of Apt1 (**A**), immobilization time of Apt2 (**B**), the concentration of Apt2 (**C**), and binding time of leptin (**D**) on the DPV signal of the α-naphthol

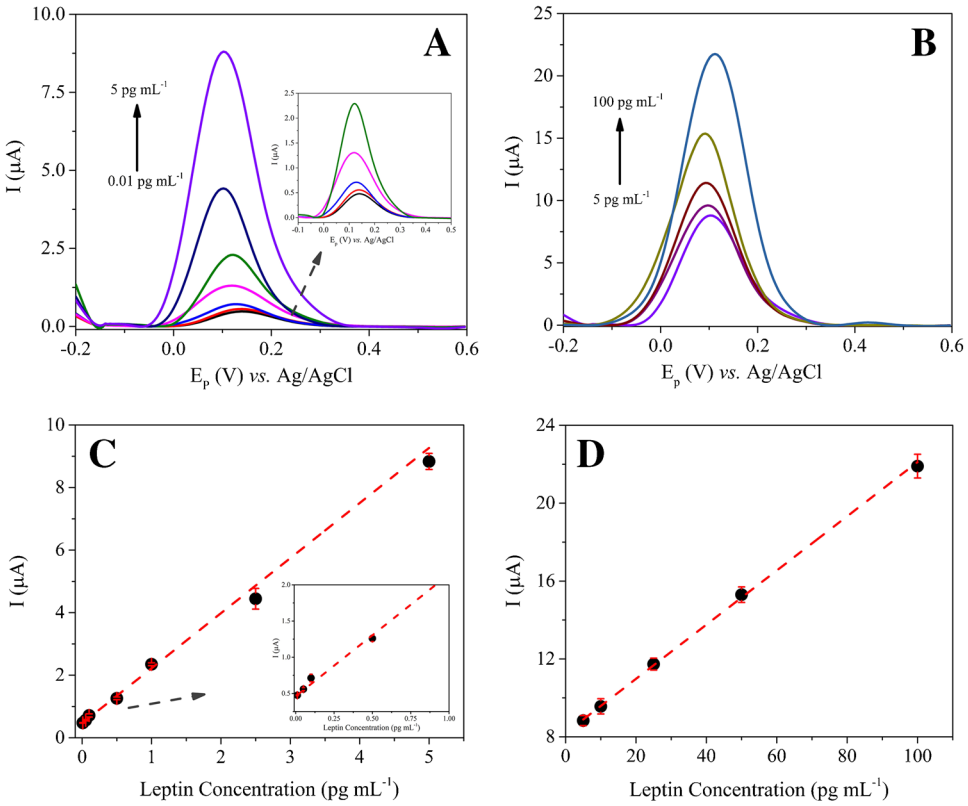

Fig. 6 DP voltammograms of increasing concentrations of leptin **A** from 0.01 to 5.0 pg mL^{-1}, **B** from 5.0 to 100.0 pg mL^{-1}, and linear regressions of leptin concentration on the α-naphthol signals at Apt2/leptin/Apt1/Au NPs/ ZnO NPs/SPE C) from 0.01 to 5.0 pg mL^{-1}, **D** from 5.0 to 100.0 pg mL^{-1}

Table 1 Summary and comparison of developed biosensors for detection of leptin

Measurement principle	Electrode	Surface architecture	Biorecognition elements	Linear range (pg mL^{-1})	LOD (pg mL^{-1})	Stability of sensor	Real samples	Ref.
Electrochemical immunosensor, $[Fe(CN)_6]^{3-/4-}$ redox solution	GCE	Glu/AuNPs/PG-BP	Antibody	0.150–2500	0.036	7 days	Human serum	[53]
Electrochemical biosensor, the signal was generated by the reaction of ALP with the α-naphthyl phosphate	GCE	SWCNTs/CS	Antibody	0–1000	1.5	–	Human serum	[54]
Electrochemical immunosensor, a signal of α-naphthol formed in the enzyme reaction catalyzed by ALP upon α-naphthyl phosphate addition	SPCE	Strept-MBs	Antibody	5–100	0.5	~ 1 month	Human serum and breast milk	[55]
Electrochemical immunosensor, $[Fe(CN)_6]^{3-/4-}$ redox solution	SPE	EDC/NHS/MPA/ $Au/Ce_3NbO_7/CeO_2$	Antibody	0.5–12, 000	0.138	7 days	Human plasma	[56]
Electrochemical immunosensor, $[Fe(CN)_6]^{3-/4-}$ redox solution	GP	EDC-NHS/PGA	Antibody	0.2–20	0.00813	8 weeks	Human serum	[57]
Biomimetic electrochemical sensor, $[Fe(CN)_6]^{3-/4-}$ redox solution	GWE	PP/MIP	–	1000–32,000	110	~ 6 months	Human serum	[49]
Electrochemical immunosensor, in 0.01 M PBS	GCE	Protein G/PPy/PPa/Au	Antibody	$1x10^4$–$1x10^8$	$1x10^4$	-	Human serum	[50]
Amperometric immunosensor, a signal of α-naphthol formed in the enzyme reaction catalyzed by ALP upon α-naphthyl phosphate addition	GCE	SWNTs/CS	Antibody	50–$5x10^5$	30	–	Human serum	[51]
Chemiluminescence immunosensor, in 5 mM luminol and 50 mM H_2O_2	Optical glass	Fe_3O_4/polydopamine/Au	Antibody	1–800	0.3	–	Human serum	[52]
Chemiluminescence immunosensor, in 5 mM luminol, and 75 mM H_2O_2	96-well plates	Hemin/G-quadruplex DNAzymes	Antibody	10–1000	1.9	30 days	Human serum	[60]
ELISA-based electrochemical biosensor, in *o*PD solution	SPGE	DTSSP	Antibody	100–20,000	33	18 days	Mice plasma	[58]
Fluorescence aptasensor	–	Adaptor*–aptamer complexes	Aptamer	10–1000	10	–	Human saliva	[59]
Electrochemical aptasensor, $[Fe(CN)_6]^{3-/4-}$ redox solution	SPE	Au NPs/TiO_2 NPs	Aptamer	1–1000	0.312	10 days	Human serum and human plasma	[23]
Electrochemical aptasensor, a signal of α-naphthol formed in the enzyme reaction catalyzed by ALP upon α-naphthyl phosphate addition	SPE	Au NPs/ZnO NPs	Aptamer	0.01–100	0.0035	15 days	Human serum and human plasma	This study

Au: gold, BP: black phosphorus, Ce_3NbO_7: cerium niobate, CeO_2: cerium oxide, CS: chitosan, DTSSP: 3,30-dithiobis (sulfosuccinimidyl propionate), EDC-NHS: N-(3-dimethylaminopropyl)-N-ethyl carbodiimide hydrochloride (EDC) and N-hydroxysuccinimide (NHS), GCE: glassy carbon electrode, Glu: glutaraldehyde, MPA: 3-mercatopropionic acid, GP: graphite paper, GWE: gold working electrode, MIP: molecularly imprinted polymer, NPs: nanoparticles, *o*PD: *o*-phenylenediamin, PBS: phosphate buffered saline, PG: porous graphene, PGA: polyglutamic acid, PP: polyphenol, PPa: pyrrole propylic acid, PPy: polypyrrole, SPCE: screen-printed carbon electrodes, SPGE: screen-printed gold electrode, Strept-MB: streptavidin-functionalized magnetic beads, SWCNTs: single-walled carbon nanotubes, TiO_2: titanium dioxide

*The adaptor is designed to have 100 bp from the green fluorescent protein (GFP) gene with an extra 26 bp for aptamer binding, while the complex sequence is designed to contain the forward adaptor sequence and the reverse aptamer sequence

low leptin levels, the local concentration at the electrode surface is rapidly depleted as the α-naphthyl phosphate substrate rapidly converts to α-naphthol due to increased diffusion effects, and results in higher sensitivity of the sensor response. On the other hand, at higher leptin levels, the enzyme is given substrate for a more extended period; therefore, the enzymatic reaction proceeds for a prolonged time. Thus, a lower slope can be exhibited with the possibility of the formed reaction products contaminating the electrode surface. Moreover, the reaction at higher target concentrations begins to reach a saturation level, as described in Michaelis-Menten type enzyme kinetics. In this study, the limit of detection (LOD) and limit of quantification (LOQ) were determined by the obtained first linear range. The LOD and LOQ values were found as 0.0035 pg mL^{-1} and 0.01 pg mL^{-1}, respectively. LOD and LOQ values were calculated with the [n*S/m] equation which has n as a constant (n is accepted as 3 in LOD and as 10 in LOQ), S is the standard deviation, and m is the slope of the calibration curve [10, 37].

Different analytical methods mainly based on electrochemical sensors for detecting leptin have been reported in previous studies. Electrochemical sensors based on EIS, amperometric, and chemiluminescence methods which are used various nanomaterials such as single-walled carbon nanotubes, pyrrole, polydopamine, and iron(II,III) oxide have been proposed for the detection of leptin [49–52]. While leptin was determined up to 30 pg mL^{-1} using the developed electrochemical sensors, it was determined at the level of 0.3 pg mL^{-1} by the chemiluminescence method. Moreover, immunoassay-based analytical techniques such as electrochemical immunosensors [53–57] and enzyme-linked immunosorbent assays (ELISA) [58] have been commonly described to detect leptin. In which antibodies and enzymes are used, these methods enabled the determination of leptin at the levels of 0.00813 to 5 pg mL^{-1}. However, these methods have some shortcomings, such as low sensitivity, low accuracy, high cost, sensitivity to environmental factors such as temperature and pH, low stability, and low shelf life. The results highlight the significantly improved superiority of this developed aptasensor over other proposed methods in a linear concentration range, LOD, and low cost.

In addition, two different aptasensors have been developed to detect leptin, one based on fluorescence [59] and the other based on label-free electrochemical [23]. In these methods, the LOD was 10 pg mL^{-1} and 0.312 pg m^{-1}, respectively. Moreover, research studies based on electrochemical methods and biosensors in leptin sensing were summarized in Table 1. Characteristics of each sensor were summarized to highlight the complexity of design and performance of the various sensors. In conclusion, it can be said that the signal amplification strategy and sandwich assay technology used in the developed simplest aptasensor, utilizing only metallic NPs, exhibit an essential role in improving the sensitivity of the aptasensor.

Real samples analysis using the developed aptasensor

The developed aptasensor was successfully used to determine leptin content in real samples. Before analysis, serum and plasma samples were diluted at 1:10. Then, leptin standard solutions at three concentrations, 0.5, 5.0, and 50.0 pg mL^{-1}, were injected into serum and plasma samples according to the standard addition method. Leptin amounts were analyzed by the developed aptasensor under optimal conditions. The measured results are presented in Table 2. Recovery% values for human serum and plasma samples were found in 96.31–103.49% (RSDs: 7.71–9.90%), 97.80–108.79% (RSDs: 7.26–9.94%), respectively, using the developed aptasensor. The analytical results demonstrated the reliability and validity and have a simple sample preparation procedure of the developed aptasensor.

Investigation of selectivity, stability, and reproducibility of the leptin aptasensor

Selectivity is one of the most indispensable parameters of an analytical method. The selectivity of the developed aptasensor was evaluated after incubating the mixtures containing 2.5 pg mL^{-1} Leptin and 250 pg mL^{-1} of each of HSA, BSA, L-Lysine, haptoglobin, dopamine, ascorbic acid, and paracetamol. As shown in Fig. 7A, 2.5 pg mL^{-1} leptin responded 5 μA, while the current signals were obtained in the presence of leptin, HSA, BSA, L-lysine, haptoglobin, and dopamine, ascorbic acid, and paracetamol were between 4.37 and 4.90 μA. These results showed that the developed aptasensor practically was not

Table 2 Recovery results using the developed aptasensor in real samples

Sample	Added amount (pg mL^{-1})	Found amount (pg mL^{-1})	Recovery %	RSD%
Human serum	0.5	0.48	96.31	9.90
	5.0	5.11*	102.15	8.97
		5.17**	103.49	8.67
	50.0	50.60	101.19	7.71
Human plasma	0.5	0.54	108.79	9.94
	5.0	5.12*	102.39	8.53
		5.32**	106.40	8.88
	50.0	48.90	97.80	7.26

*Obtained from first calibration curve

**Obtained from second calibration curve

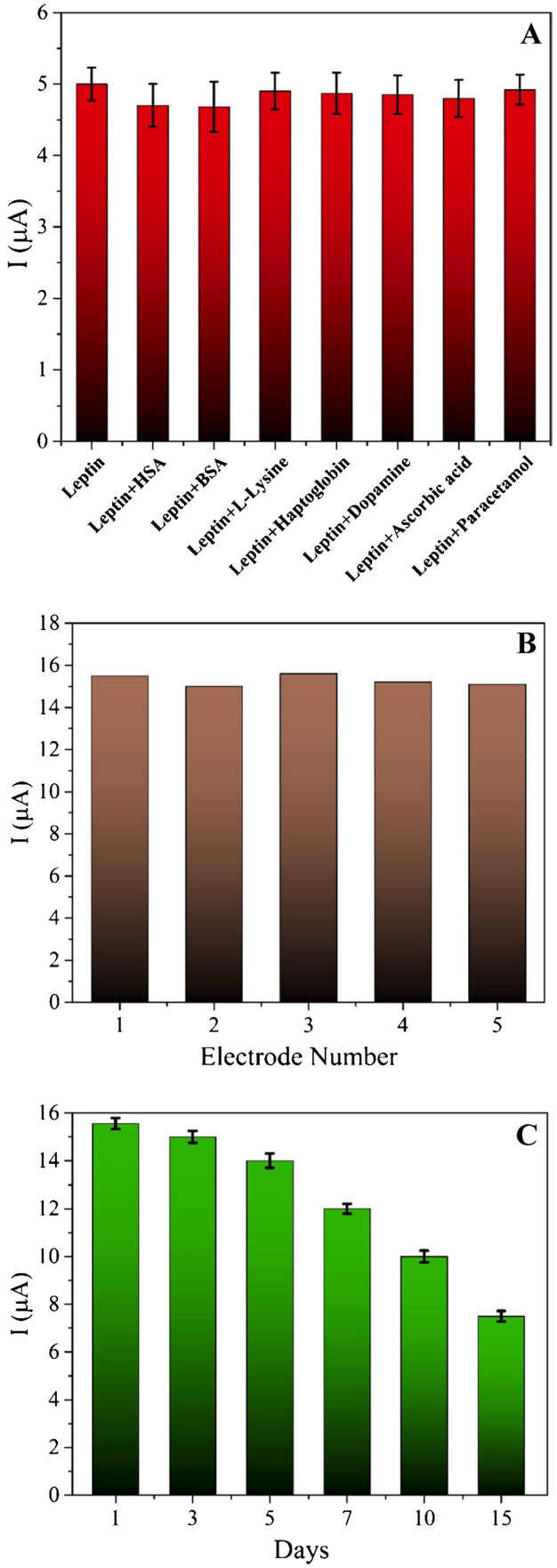

◂ **Fig. 7** Selectivity of the developed aptasensor to leptin by comparing it to the different interfering compounds (**A**), reproducibility of the developed aptasensor using five different electrodes (**B**), and stability of the developed aptasensor (**C**)

affected by interfering compounds to detect leptin, indicating the high selectivity (DP voltammograms are presented in Fig. S4). Moreover, after incubation of 50.0 pg mL^{-1} leptin to the aptasensor, the reproducibility of the developed aptasensor was evaluated according to the current responses obtained from five different aptasensors prepared under optimum conditions (Fig. 7B). The results showed that the developed aptasensor exhibited a high reproducibility with 1.5% RSD (DP voltammograms are presented in Fig. S5).

In addition, the developed aptasensor was stored in a +4°C refrigerator for 15 days, and its stability against leptin response was investigated. DPV responses could remain as 96.4%, 90.0%, 77.1%, 64.3%, and 48.2% on days 1, 3, 5, 7, 10 ,and 15 (Fig. 7C) compared to the day of initial preparation (DP voltammograms are presented in Fig. S6). As can be seen in Table 1, the results revealed the excellent stability of the developed aptasensor. Compared to antibody-based immunosensors and fluorescent sensors. However, its stability concerning polymeric nanomaterials modified sensors needs to be improved.

Conclusion

To sum up, a novel aptasensor was developed for the ultrasensitive detection of leptin using the enzyme-labeled electrochemical method for the first time. The prepared ZnO NPs/Au NPs/SPE sensor efficiently loaded aptamer molecules according to the layer-by-layer strategy. Under optimal conditions, the electroactive product α-naphthol was used as a sensing substrate, and a wide linear calibration range varied from 0.01 to 100.0 pg mL^{-1} and a low detection limit of 0.0035 pg mL^{-1} was obtained. Previous studies found plasma leptin concentrations in the range of 19.2 ± 6.6ng mL^{-1} and 12.5 ± 6.9 ng mL^{-1} for the early period of deterioration and in children with traumatic brain injury, respectively [61, 62]. Therefore, the results showed that the designed aptasensor is a favorable sensor for detecting leptin in neurodegenerative diseases. Moreover, the developed aptasensor provided superior selectivity, stability, and reproducibility to detect leptin in human biological samples. Additionally, the fact that the developed aptasensor is as sensitive as the immunosensor and the use of aptamers, which are more economical biorecognition elements than antibodies, will draw attention to the superior features of the aptasensor.

Supplementary Information The online version contains supplementary material available at https://doi.org/10.1007/s00604-022-05487-z.

Acknowledgements This work was produced from the PhD thesis of Cem Erkmen (Ankara University, Health Sciences Institute). The Council of Higher Education (YOK) was greatly appreciated for providing scholarships under the special 100/2000 scholarship program to Cem Erkmen. Cem Erkmen also thanks to the financial support from The Scientific and Technological Research Council of Türkiye (TUBITAK) under the BIDEB/2211-A doctoral scholarship program. The authors acknowledge The Scientific and Technological Research Council of Türkiye (TUBITAK, project no.: 122Z695) for financial support.

Declarations

Competing interests The authors declare no competing interests.

References

1. McAllister TW (2011) Neurobiological consequences of traumatic brain injury. Dialogues Clin Neurosci 13. https://doi.org/10.31887/dcns.2011.13.2/tmcallister
2. Bouchard HC, Sun D, Dennis EL et al (2022) Age-dependent white matter disruptions after military traumatic brain injury: multivariate analysis results from ENIGMA brain injury. Hum Brain Mapp. https://doi.org/10.1002/hbm.25811
3. Mollayeva T, Mollayeva S, Colantonio A (2018) Traumatic brain injury: sex, gender and intersecting vulnerabilities. Nat Rev Neurol 14(12):711–722. https://doi.org/10.1038/s41582-018-0091-y
4. Daoud H, Alharfi I, Alhelali I et al (2014) Brain injury biomarkers as outcome predictors in pediatric severe traumatic brain injury. Neurocrit Care 20. https://doi.org/10.1007/s12028-013-9879-1
5. Jiang W, Zou W, Hu M, et al (2022) Hydrogen sulphide attenuates neuronal apoptosis of substantia nigra by re-establishing autophagic flux via promoting leptin signalling in a 6-hydroxydopamine rat model of Parkinson's disease. Clin Exp Pharmacol Physiol 49. https://doi.org/10.1111/1440-1681.13587
6. Toklu HZ, Yang Z, Oktay S, et al (2018) Overpressure blast injury-induced oxidative stress and neuroinflammation response in rat frontal cortex and cerebellum. Behav Brain Res 340. https://doi.org/10.1016/j.bbr.2017.04.025
7. Wang S, Yan X, Yang Y et al (2021) Advances and perspectives of aptasensors for the detection of tetracyclines: a class of model compounds of food analysis. Food Chem 364:130361. https://doi.org/10.1016/j.foodchem.2021.130361
8. Zhang N, Li J, Liu B et al (2022) Signal enhancing strategies in aptasensors for the detection of small molecular contaminants by nanomaterials and nucleic acid amplification. Talanta 236:122866. https://doi.org/10.1016/j.talanta.2021.122866
9. Melinte G, Selvolini G, Cristea C, Marrazza G (2021) Aptasensors for lysozyme detection: Recent advances. Talanta 226:122169. https://doi.org/10.1016/j.talanta.2021.122169
10. Bozal-Palabiyik B, Uslu B, Marrazza G (2019) Nanosensors in biomarker detection. In: New Developments in nanosensors for pharmaceutical analysis. https://doi.org/10.1016/B978-0-12-816144-9.00011-0
11. He B, Dong X (2019) Hierarchically porous Zr-MOFs labelled methylene blue as signal tags for electrochemical patulin aptasensor based on ZnO nano flower. Sensors Actuators, B Chem 294. https://doi.org/10.1016/j.snb.2019.05.045
12. Yang SL, Li G, Feng J, et al (2022) Synthesis of core/satellite donut-shaped ZnO–Au nanoparticles incorporated with reduced graphene oxide for electrochemical sensing of rutin. Electrochim Acta 412. https://doi.org/10.1016/j.electacta.2022.140157
13. Kenarkob M, Pourghobadi Z (2019) Electrochemical sensor for acetaminophen based on a glassy carbon electrode modified with ZnO/Au nanoparticles on functionalized multi-walled carbon nano-tubes. Microchem J 146. https://doi.org/10.1016/j.microc.2019.02.038
14. Rovina K, Siddiquee S (2016) Electrochemical sensor based rapid determination of melamine using ionic liquid/zinc oxide nanoparticles/chitosan/gold electrode. Food Control 59. https://doi.org/10.1016/j.foodcont.2015.07.009
15. Ezhil Vilian AT, Kang SM, Yeong Oh S et al (2020) A simple strategy for the synthesis of flower-like textures of Au-ZnO anchored carbon nanocomposite towards the high-performance electrochemical sensing of sunset yellow. Food Chem 323. https://doi.org/10.1016/j.foodchem.2020.126848
16. Fang L, Huang K, Zhang B, et al (2014) Nanosheet-based 3D hierarchical ZnO structure decorated with Au nanoparticles for enhanced electrochemical detection of dopamine. RSC Adv 4. https://doi.org/10.1039/c4ra06090c
17. Madhu R, Dinesh B, Chen SM et al (2015) An electrochemical synthesis strategy for composite based ZnO microspheres-Au nanoparticles on reduced graphene oxide for the sensitive detection of hydrazine in water samples. RSC Adv 5. https://doi.org/10.1039/c5ra05612h
18. Wang M, Fu Z, Li B, et al (2014) One-step, ultrasensitive, and electrochemical assay of microRNAs based on t7 exonuclease assisted cyclic enzymatic amplification. Anal Chem 86. https://doi.org/10.1021/ac5010376
19. Wen Y, Pei H, Shen Y, et al (2012) DNA Nanostructure-based ınterfacial engineering for PCR-free ultrasensitive electrochemical analysis of microRNA. Sci Rep 2. https://doi.org/10.1038/srep00867
20. Yang H (2012) Enzyme-based ultrasensitive electrochemical biosensors. Curr Opin Chem Biol 16(3–4):422–428. https://doi.org/10.1016/j.cbpa.2012.03.015
21. Melinte G, Hosu O, Ștefan G, et al (2022) Poly-L-Lysine@gold nanostructured hybrid platform for Lysozyme aptamer sandwich-based detection. Electrochim Acta 403. https://doi.org/10.1016/j.electacta.2021.139718
22. Ashley J, Li SFY (2013) Three-dimensional selection of leptin aptamers using capillary electrophoresis and implications for clone validation. Anal Biochem 434:146–152. https://doi.org/10.1016/j.ab.2012.11.024
23. ERKMEN C, TIĞ GA, USLU B (2022) First label-free impedimetric aptasensor based on Au NPs/TiO2 NPs for the determination of leptin. Sensors Actuators B Chem 358. https://doi.org/10.1016/j.snb.2022.131420
24. Rasheed PA, Sandhyarani N (2017) Electrochemical DNA sensors based on the use of gold nanoparticles: a review on recent developments. Microchim Acta 184:981–1000. https://doi.org/10.1007/s00604-017-2143-1
25. Srujana S, Bhagat D (2022) Chemical-based synthesis of ZnO nanoparticles and their applications in agriculture. Nanotechnol Environ Eng 7. https://doi.org/10.1007/s41204-022-00224-6
26. Prabhu K, Malode SJ, Shetti NP, Kulkarni RM (2022) Analysis of herbicide and its applications through a sensitive electrochemical technique based on MWCNTs/ZnO/CPE fabricated sensor. Chemosphere 287. https://doi.org/10.1016/j.chemosphere.2021.132086

27. Svigelj R, Zuliani I, Grazioli C et al (2022) An effective label-free electrochemical aptasensor based on gold nanoparticles for gluten detection. Nanomaterials 12. https://doi.org/10.3390/nano12060987
28. Chen H, Wang Y, Li X, et al (2018) A CO2-tunable plasmonic nanosensor based on the interfacial assembly of gold nanoparticles on diblock copolymers grafted from gold surfaces. RSC Adv 8. https://doi.org/10.1039/c8ra02934b
29. Jafari S, Dehghani M, Nasirizadeh N, et al (2019) Label-free electrochemical detection of Cloxacillin antibiotic in milk samples based on molecularly imprinted polymer and graphene oxide-gold nanocomposite. Meas J Int Meas Confed 145. https://doi.org/10.1016/j.measurement.2019.05.068
30. Srivastava M, Nirala NR, Srivastava SK, Prakash R (2018) A comparative study of aptasensor vs ımmunosensor for label-free PSA Cancer detection on GQDs-AuNRs modified screen-printed electrodes. Sci Rep 8. https://doi.org/10.1038/s41598-018-19733-z
31. Nazari M, Kashanian S, Rafipour R, Omidfar K (2019) Biosensor design using an electroactive label-based aptamer to detect bisphenol A in serum samples. J Biosci 44. https://doi.org/10.1007/s12038-019-9921-3
32. Nia NG, Azadbakht A (2018) Nanostructured aptamer-based sensing platform for highly sensitive recognition of myoglobin. Microchim Acta 185. https://doi.org/10.1007/s00604-018-2860-0
33. Muhammad A, Yusof NA, Hajian R, Abdullah J (2016) Construction of an electrochemical sensor based on carbon nanotubes/gold nanoparticles for trace determination of amoxicillin in bovine milk. Sensors (Switzerland) 16. https://doi.org/10.3390/s16010056
34. Saeb E, Asadpour-Zeynali K (2021) Facile synthesis of TiO2@PANI@Au nanocomposite as an electrochemical sensor for determination of hydrazine. Microchem J 160:105603. https://doi.org/10.1016/j.microc.2020.105603
35. Salih E, Mekawy M, Hassan RYA, El-Sherbiny IM (2016) Synthesis, characterization and electrochemical-sensor applications of zinc oxide/graphene oxide nanocomposite. J Nanostructure Chem 6. https://doi.org/10.1007/s40097-016-0188-z
36. Heydari M, Ghoreishi SM, Khoobi A (2019) Chemometrics-assisted determination of Sudan dyes using zinc oxide nanoparticle-based electrochemical sensor. Food Chem 283. https://doi.org/10.1016/j.foodchem.2018.12.132
37. Kurbanoglu S, Ozkan SA (2018) Electrochemical carbon based nanosensors: a promising tool in pharmaceutical and biomedical analysis. J Pharm Biomed Anal 147:439–457. https://doi.org/10.1016/j.jpba.2017.06.062
38. García-González R, Fernández Abedul MT (2020) Electrochemical impedance spectroscopy for characterization of electrode surfaces. In: Laboratory methods in dynamic electroanalysis. https://doi.org/10.1016/B978-0-12-815932-3.00012-7
39. Nodehi M, Baghayeri M, Behazin R, Veisi H (2021) Electrochemical aptasensor of bisphenol A constructed based on 3D mesoporous structural SBA-15-Met with a thin layer of gold nanoparticles. Microchem J 162. https://doi.org/10.1016/j.microc.2020.105825
40. Guo S, Wang E (2007) Synthesis and electrochemical applications of gold nanoparticles. Anal Chim Acta 598(2):181–192. https://doi.org/10.1016/j.aca.2007.07.054
41. Shi L, Wang Z, Bai L, Yang G (2022) Preparation of 3d nanoflower-like ZnO/graphene oxide decorated with Au@AuPt Bimetallic nanoparticles for electrochemical determination of doxorubicin hydrochloride. Int J Electrochem Sci 17. https://doi.org/10.20964/2022.1.45
42. Li F, Gao X, Wang X, et al (2022) Ultrasensitive sandwich RNA-aptasensor based on dual-signal amplification strategy for highly sensitive neomycin detection. Food Control 131. https://doi.org/10.1016/j.foodcont.2021.108445
43. Wang Y, Wang Y, Wang F et al (2022) Electrochemical aptasensor based on gold modified thiol graphene as sensing platform and gold-palladium modified zirconium metal-organic frameworks nanozyme as signal enhancer for ultrasensitive detection of mercury ions. J Colloid Interface Sci 606. https://doi.org/10.1016/j.jcis.2021.08.055
44. Liu J, Zhu B, Dong H et al (2022) A novel electrochemical insulin aptasensor: from glassy carbon electrodes to disposable, single-use laser-scribed graphene electrodes. Bioelectrochemistry 143. https://doi.org/10.1016/j.bioelechem.2021.107995
45. Martins TS, Bott-Neto JL, Oliveira ON, Machado SAS (2022) A sandwich-type electrochemical immunosensor based on Au-rGO composite for CA15-3 tumor marker detection. Microchim Acta 189. https://doi.org/10.1007/s00604-021-05145-w
46. Gasparotto G, Costa JPC, Costa PI et al (2017) Electrochemical immunosensor based on ZnO nanorods-Au nanoparticles nanohybrids for ovarian cancer antigen CA-125 detection. Mater Sci Eng C 76:1240–1247. https://doi.org/10.1016/j.msec.2017.02.031
47. Gholizadeh A, Shahrokhian S, Iraji Zad A, et al (2012) Fabrication of sensitive glutamate biosensor based on vertically aligned CNT nanoelectrode array and investigating the effect of CNTs density on the electrode performance. Anal Chem 84. https://doi.org/10.1021/ac300463x
48. Zhou Y, Liu J, Dong H, et al (2022) Target-induced silver nanocluster generation for highly sensitive electrochemical aptasensor towards cell-secreted interferon-γ. Biosens Bioelectron 203. https://doi.org/10.1016/j.bios.2022.114042
49. Mihailescu CM, Stan D, Savin M et al (2020) Platform with biomimetic electrochemical sensors for adiponectin and leptin detection in human serum. Talanta 210:120643. https://doi.org/10.1016/j.talanta.2019.120643
50. Chen W, Lei Y, Li CM (2010) Regenerable leptin immunosensor based on protein G immobilized au-pyrrole propylic acid-polypyrrole nanocomposite. Electroanalysis 22:1078–1083. https://doi.org/10.1002/elan.200900536
51. Dong F, Luo R, Chen H et al (2014) Amperometric immunosensor based on carbon nanotubes/chitosan film modified electrodes for detection of human leptin. Int J Electrochem Sci 9:6924–6935
52. He Y, Sun J, Wang X, Wang L (2015) Detection of human leptin in serum using chemiluminescence immunosensor: signal amplification by hemin/G-quadruplex DNAzymes and protein carriers by Fe3O4/polydopamine/Au nanocomposites. Sensors Actuators B Chem 221:792–798. https://doi.org/10.1016/j.snb.2015.07.022
53. Cai J, Gou X, Sun B et al (2019) Porous graphene-black phosphorus nanocomposite modified electrode for detection of leptin. Biosens Bioelectron 137:88–95. https://doi.org/10.1016/j.bios.2019.04.045
54. Zhang Q, Qing Y, Huang X et al (2018) Synthesis of single-walled carbon nanotubes–chitosan nanocomposites for the development of an electrochemical biosensor for serum leptin detection. Mater Lett 211:348–351. https://doi.org/10.1016/j.matlet.2017.10.036
55. Ojeda I, Moreno-Guzmán M, González-Cortés A et al (2013) A disposable electrochemical immunosensor for the determination of leptin in serum and breast milk. Analyst 138:4284–4291. https://doi.org/10.1039/c3an00183k
56. Liu X, Tseng CL, Lin LY et al (2021) Template-free synthesis of mesoporous Ce3NbO7/CeO2 hollow nanospheres for label-free electrochemical immunosensing of leptin. Sensors Actuators, B Chem 341:130005. https://doi.org/10.1016/j.snb.2021.130005

57. Özcan B, Sezgintürk MK (2021) A novel and disposable GP-based impedimetric biosensor using electropolymerization process with PGA for highly sensitive determination of leptin: Early diagnosis of childhood obesity. Talanta 225. https://doi.org/10.1016/j.talanta.2020.121985
58. Sung R, Seok Heo Y (2021) Sandwich elisa-based electrochemical biosensor for leptin in control and diet-induced obesity mouse model. Biosensors 11:1–9. https://doi.org/10.3390/bios11010007
59. Cavallo FR, Mirza KB, De Mateo S et al (2021) Aptasensor for quantification of leptin through pCR amplification of short DNA-aptamers. ACS Sensors 6:709–715. https://doi.org/10.1021/acssensors.0c02605
60. He Y, Wang X, Zhang Y et al (2013) An ultrasensitive chemiluminescent immunosensor for the detection of human leptin using hemin/G-quadruplex DNAzymes-assembled signal amplifier. Talanta 116:816–821. https://doi.org/10.1016/j.talanta.2013.07.074
61. Du Q, Yang DB, Shen YF, et al (2013) Plasma leptin level predicts hematoma growth and early neurological deterioration after acute intracerebral hemorrhage. Peptides 45. https://doi.org/10.1016/j.peptides.2013.04.017
62. Lin C, Huang SJ, Wang N, Shen ZP (2012) Relationship between plasma leptin levels and clinical outcomes of pediatric traumatic brain injury. Peptides 35:166–171. https://doi.org/10.1016/j.peptides.2012.03.024